Article

Observation of New Properties of Secondary Cosmic Rays Lithium, Beryllium, and Boron by the Alpha Magnetic Spectrometer on the International Space Station

AMS Collaboration

AZZARELLO, Philipp (Collab.), *et al*.

Abstract

We report on the observation of new properties of secondary cosmic rays Li, Be, and B measured in the rigidity (momentum per unit charge) range 1.9 GV to 3.3 TV with a total of 5.4×10^6 nuclei collected by AMS during the first five years of operation aboard the International Space Station. The Li and B fluxes have an identical rigidity dependence above 7 GV and all three fluxes have an identical rigidity dependence above 30 GV with the Li/Be flux ratio of 2.0±0.1. The three fluxes deviate from a single power law above 200 GV in an identical way. This behavior of secondary cosmic rays has also been observed in the AMS measurement of primary cosmic rays He, C, and O but the rigidity dependences of primary cosmic rays and of secondary cosmic rays are distinctly different. In particular, above 200 GV, the secondary cosmic rays harden more than the primary cosmic rays.

Reference

AMS Collaboration, AZZARELLO, Philipp (Collab.), *et al*. Observation of New Properties of Secondary Cosmic Rays Lithium, Beryllium, and Boron by the Alpha Magnetic Spectrometer on the International Space Station. *Physical Review Letters*, 2018, vol. 120, no. 2, p. 021101

DOI : 10.1103/PhysRevLett.120.021101

Editors' Suggestion | Featured in Physics

Observation of New Properties of Secondary Cosmic Rays Lithium, Beryllium, and Boron by the Alpha Magnetic Spectrometer on the International Space Station

M. Aguilar,[27] L. Ali Cavasonza,[1] G. Ambrosi,[32] L. Arruda,[25] N. Attig,[22] S. Aupetit,[18] P. Azzarello,[17] A. Bachlechner,[1] F. Barao,[25] A. Barrau,[18] L. Barrin,[16] A. Bartoloni,[37] L. Basara,[35] S. Başeğmez-du Pree,[6] M. Battarbee,[45] R. Battiston,[35,36,*] U. Becker,[10] M. Behlmann,[10] B. Beischer,[1] J. Berdugo,[27] B. Bertucci,[32,33] K. F. Bindel,[23] V. Bindi,[20] W. de Boer,[23] K. Bollweg,[21] V. Bonnivard,[18] B. Borgia,[37,38] M. J. Boschini,[29] M. Bourquin,[17] E. F. Bueno,[39] J. Burger,[10] W. J. Burger,[35] F. Cadoux,[17] X. D. Cai,[10] M. Capell,[10] S. Caroff,[3] J. Casaus,[27] G. Castellini,[15] F. Cervelli,[34] M. J. Chae,[40] Y. H. Chang,[11] A. I. Chen,[10] G. M. Chen,[6] H. S. Chen,[6,7] L. Cheng,[41] H. Y. Chou,[11] E. Choumilov,[10] V. Choutko,[10] C. H. Chung,[1] C. Clark,[21] R. Clavero,[24] G. Coignet,[3] C. Consolandi,[20] A. Contin,[8,9] C. Corti,[20] W. Creus,[44] M. Crispoltoni,[32,33] Z. Cui,[41] K. Dadzie,[10] Y. M. Dai,[5] A. Datta,[20] C. Delgado,[27] S. Della Torre,[29] M. B. Demirköz,[2] L. Derome,[18] S. Di Falco,[34] F. Dimiccoli,[35,36] C. Díaz,[27] P. von Doetinchem,[20] F. Dong,[31] F. Donnini,[32,33] M. Duranti,[32] D. D'Urso,[32,†] A. Egorov,[10] A. Eline,[10] T. Eronen,[45] J. Feng,[10] E. Fiandrini,[32,33] P. Fisher,[10] V. Formato,[32] Y. Galaktionov,[10] G. Gallucci,[34] R. J. García-López,[24] C. Gargiulo,[16] H. Gast,[1] I. Gebauer,[23] M. Gervasi,[29,30] A. Ghelfi,[18] F. Giovacchini,[27] D. M. Gómez-Coral,[28] J. Gong,[31] C. Goy,[3] V. Grabski,[28] D. Grandi,[29] M. Graziani,[23] K. H. Guo,[19] S. Haino,[44] K. C. Han,[26] Z. H. He,[19] M. Heil,[10] T. H. Hsieh,[10] H. Huang,[44,‡] Z. C. Huang,[19] C. Huh,[14] M. Incagli,[34] M. Ionica,[32] W. Y. Jang,[14] Yi Jia,[10] H. Jinchi,[26] S. C. Kang,[14] K. Kanishev,[35,16] B. Khiali,[11] G. N. Kim,[14] K. S. Kim,[14] Th. Kirn,[1] C. Konak,[2] O. Kounina,[10] A. Kounine,[10] V. Koutsenko,[10] A. Kulemzin,[10] G. La Vacca,[29,30] E. Laudi,[16] G. Laurenti,[8] I. Lazzizzera,[35,36] A. Lebedev,[10] H. T. Lee,[43] S. C. Lee,[44] C. Leluc,[17] H. S. Li,[42] J. Q. Li,[31] Q. Li,[31] T. X. Li,[19] Y. Li,[17,§] Z. H. Li,[6] Z. Y. Li,[44,§] S. Lim,[14] C. H. Lin,[44] P. Lipari,[37] T. Lippert,[22] D. Liu,[11] Hu Liu,[10,‖] V. D. Lordello,[39] S. Q. Lu,[44,§] Y. S. Lu,[6] K. Luebelsmeyer,[1] F. Luo,[41] J. Z. Luo,[31] S. S. Lyu,[19] F. Machate,[1] C. Mañá,[27] J. Marín,[27] T. Martin,[21] G. Martínez,[27] N. Masi,[8] D. Maurin,[18] A. Menchaca-Rocha,[28] Q. Meng,[31] V. M. Mikuni,[39] D. C. Mo,[19] P. Mott,[21] T. Nelson,[20] J. Q. Ni,[19] N. Nikonov,[1] F. Nozzoli,[32,¶] A. Oliva,[27] M. Orcinha,[25] M. Palermo,[20] F. Palmonari,[8,9] C. Palomares,[27] M. Paniccia,[17] M. Pauluzzi,[32,33] S. Pensotti,[29,30] C. Perrina,[17] H. D. Phan,[10] N. Picot-Clemente,[13] F. Pilo,[34] C. Pizzolotto,[32,**] V. Plyaskin,[10] M. Pohl,[17] V. Poireau,[3] L. Quadrani,[8,9] X. M. Qi,[19] X. Qin,[10] Z. Y. Qu,[44,††] T. Räihä,[1] P. G. Rancoita,[29] D. Rapin,[17] J. S. Ricol,[18] S. Rosier-Lees,[3] A. Rozhkov,[10] D. Rozza,[29,30] R. Sagdeev,[12] S. Schael,[1] S. M. Schmidt,[22] A. Schulz von Dratzig,[1] G. Schwering,[1] E. S. Seo,[13] B. S. Shan,[4] J. Y. Shi,[31] T. Siedenburg,[1] D. Son,[14] J. W. Song,[41] M. Tacconi,[29,30] X. W. Tang,[6] Z. C. Tang,[6] D. Tescaro,[24] Samuel C. C. Ting,[10,16] S. M. Ting,[10] N. Tomassetti,[32,33] J. Torsti,[45] C. Türkoğlu,[2] T. Urban,[21] V. Vagelli,[32,33] E. Valente,[37,38] E. Valtonen,[45] M. Vázquez Acosta,[24] M. Vecchi,[39] M. Velasco,[27] J. P. Vialle,[3] V. Vitale,[35,¶] L. Q. Wang,[41] N. H. Wang,[41] Q. L. Wang,[5] X. Wang,[10] X. Q. Wang,[6,7] Z. X. Wang,[19] C. C. Wei,[44,‡‡] Z. L. Weng,[10] K. Whitman,[20] H. Wu,[31] X. Wu,[17] R. Q. Xiong,[31] W. Xu,[10] Q. Yan,[10] J. Yang,[40] M. Yang,[6] Y. Yang,[42] H. Yi,[31] Y. J. Yu,[5] Z. Q. Yu,[6] M. Zannoni,[29,30] S. Zeissler,[23] C. Zhang,[6] F. Zhang,[6] J. Zhang,[10,‡] J. H. Zhang,[31] S. W. Zhang,[6,7] Z. Zhang,[10] Z. M. Zheng,[4] H. L. Zhuang,[6] V. Zhukov,[1] A. Zichichi,[8,9] N. Zimmermann,[1] and P. Zuccon[10]

(AMS Collaboration)

[1]*I. Physics Institute and JARA-FAME, RWTH Aachen University, D-52056 Aachen, Germany*
[2]*Department of Physics, Middle East Technical University (METU), 06800 Ankara, Turkey*
[3]*Laboratoire d'Annecy-le-Vieux de Physique des Particules (LAPP), CNRS/IN2P3 and Université Savoie Mont Blanc, F-74941 Annecy-le-Vieux, France*
[4]*Beihang University (BUAA), Beijing 100191, China*
[5]*Institute of Electrical Engineering (IEE), Chinese Academy of Sciences, Beijing 100190, China*
[6]*Institute of High Energy Physics (IHEP), Chinese Academy of Sciences, Beijing 100049, China*
[7]*University of Chinese Academy of Sciences (UCAS), Beijing 100049, China*
[8]*INFN Sezione di Bologna, I-40126 Bologna, Italy*
[9]*Università di Bologna, I-40126 Bologna, Italy*
[10]*Massachusetts Institute of Technology (MIT), Cambridge, Massachusetts 02139, USA*
[11]*National Central University (NCU), Chung-Li, Tao Yuan 32054, Taiwan*
[12]*East-West Center for Space Science, University of Maryland, College Park, Maryland 20742, USA*
[13]*IPST, University of Maryland, College Park, Maryland 20742, USA*
[14]*CHEP, Kyungpook National University, 41566 Daegu, Korea*
[15]*CNR-IROE, I-50125 Firenze, Italy*

[16]European Organization for Nuclear Research (CERN), CH-1211 Geneva 23, Switzerland
[17]DPNC, Université de Genève, CH-1211 Genève 4, Switzerland
[18]Laboratoire de Physique Subatomique et de Cosmologie (LPSC), CNRS/IN2P3 and Université Grenoble-Alpes, F-38026 Grenoble, France
[19]Sun Yat-Sen University (SYSU), Guangzhou 510275, China
[20]Physics and Astronomy Department, University of Hawaii, Honolulu, Hawaii 96822, USA
[21]National Aeronautics and Space Administration Johnson Space Center (JSC), Jacobs Engineering, and Business Integra, Houston, Texas 77058, USA
[22]Jülich Supercomputing Centre and JARA-FAME, Research Centre Jülich, D-52425 Jülich, Germany
[23]Institut für Experimentelle Teilchenphysik, Karlsruhe Institute of Technology (KIT), D-76131 Karlsruhe, Germany
[24]Instituto de Astrofísica de Canarias (IAC), E-38205 La Laguna, and Departamento de Astrofísica, Universidad de La Laguna, E-38206 La Laguna, Tenerife, Spain
[25]Laboratório de Instrumentação e Física Experimental de Partículas (LIP), P-1000 Lisboa, Portugal
[26]National Chung-Shan Institute of Science and Technology (NCSIST), Longtan, Tao Yuan 32546, Taiwan
[27]Centro de Investigaciones Energéticas, Medioambientales y Tecnológicas (CIEMAT), E-28040 Madrid, Spain
[28]Instituto de Física, Universidad Nacional Autónoma de México (UNAM), México, D. F. 01000, Mexico
[29]INFN Sezione di Milano–Bicocca, I-20126 Milano, Italy
[30]Università di Milano-Bicocca, I-20126 Milano, Italy
[31]Southeast University (SEU), Nanjing 210096, China
[32]INFN Sezione di Perugia, I-06100 Perugia, Italy
[33]Università di Perugia, I-06100 Perugia, Italy
[34]INFN Sezione di Pisa, I-56100 Pisa, Italy
[35]INFN TIFPA, I-38123 Povo, Trento, Italy
[36]Università di Trento, I-38123 Povo, Trento, Italy
[37]INFN Sezione di Roma 1, I-00185 Roma, Italy
[38]Università di Roma La Sapienza, I-00185 Roma, Italy
[39]Instituto de Física de São Carlos, Universidade de São Paulo, CP 369, 13560-970 São Carlos, São Paulo, SP, Brazil
[40]Department of Physics, Ewha Womans University, Seoul 120-750, Korea
[41]Shandong University (SDU), Jinan, Shandong 250100, China
[42]National Cheng Kung University, Tainan 70101, Taiwan
[43]Academia Sinica Grid Center (ASGC), Nankang, Taipei 11529, Taiwan
[44]Institute of Physics, Academia Sinica, Nankang, Taipei 11529, Taiwan
[45]Space Research Laboratory, Department of Physics and Astronomy, University of Turku, FI-20014 Turku, Finland

(Received 7 November 2017; published 11 January 2018)

We report on the observation of new properties of secondary cosmic rays Li, Be, and B measured in the rigidity (momentum per unit charge) range 1.9 GV to 3.3 TV with a total of 5.4×10^6 nuclei collected by AMS during the first five years of operation aboard the International Space Station. The Li and B fluxes have an identical rigidity dependence above 7 GV and all three fluxes have an identical rigidity dependence above 30 GV with the Li/Be flux ratio of 2.0 ± 0.1. The three fluxes deviate from a single power law above 200 GV in an identical way. This behavior of secondary cosmic rays has also been observed in the AMS measurement of primary cosmic rays He, C, and O but the rigidity dependences of primary cosmic rays and of secondary cosmic rays are distinctly different. In particular, above 200 GV, the secondary cosmic rays harden more than the primary cosmic rays.

DOI: 10.1103/PhysRevLett.120.021101

Lithium, beryllium, and boron nuclei in cosmic rays are thought to be produced by the collisions of nuclei with the interstellar medium [1]. They are called secondary cosmic rays. Over the last 50 years, only a few experiments have measured the lithium [2–4] and beryllium [2–6] fluxes in cosmic rays above a few GV. Typically, these measurements have errors larger than 50% at 100 GV. For the boron flux, measurements [2–11] have errors larger than 15% at 100 GV.

Precise measurements of primary cosmic rays, protons, helium, carbon, and oxygen, by AMS [12–14] have shown a hardening of all their spectra above 200 GV. In addition, above 60 GV, the spectra of He, C, and O were found to have

an identical rigidity dependence. The detailed knowledge of lithium, beryllium, and boron fluxes rigidity dependences is important to study the origin of the hardening in cosmic ray fluxes. There are many theoretical models describing the behavior of cosmic rays. For example, if the hardening in cosmic rays is related to the injected spectra at their source, then similar hardening is expected both for secondary and primary cosmic rays [15]. However, if the hardening is related to propagation properties in the Galaxy then a stronger hardening is expected for the secondary with respect to the primary cosmic rays [16]. The theoretical models have their limitations, as none of them predicted the observed spectral behavior of the primary cosmic rays He, C, and O. Furthermore, none of the theoretical models predict the observed spectral behavior of the secondary cosmic rays Li, Be, and B reported in this Letter.

In this Letter we report the precise measurement of the lithium, beryllium, and boron fluxes in cosmic rays in the rigidity range from 1.9 GV to 3.3 TV. This measurement is based on 1.9×10^6 lithium, 0.9×10^6 beryllium, and 2.6×10^6 boron nuclei collected by AMS during the first 5 y (May 19, 2011 to May 26, 2016) of operation aboard the International Space Station (ISS). The total error on each of the fluxes is 3%–4% in the 100–108 GV bin.

Detector.—The layout and description of the AMS detector are presented in Ref. [17]. The key elements used in this measurement are the permanent magnet [18], the silicon tracker [19], and the four planes of time of flight (TOF) scintillation counters [20]. Further information on the layout and the performance of the silicon tracker and the TOF is included in Ref. [21], see also Ref. [22]. AMS also contains a transition radiation detector (TRD), a ring imaging Čerenkov detector (RICH), an electromagnetic calorimeter (ECAL), and an array of 16 anticoincidence counters.

Li, Be, and B nuclei traversing AMS were triggered as described in detail in Ref. [13]. The trigger efficiencies for $3 \leq Z \leq 5$ events were measured to be $> 98\%$ over the entire rigidity range.

Monte Carlo (MC) simulated events were produced using a dedicated program developed by the collaboration based on the GEANT-4.10.1 package [23]. The program simulates electromagnetic and hadronic interactions of particles in the material of AMS and generates detector responses. The Glauber-Gribov model [23] tuned to reproduce the AMS helium data, see Fig. SM 1(a),1(b) in Ref. [13], was used for the description of the nuclei inelastic cross sections. The Monte Carlo event samples have sufficient statistics such that they do not contribute to the errors.

Event selection.—In the first five years AMS has collected 8.5×10^{10} cosmic ray events. The collection time used in this analysis includes only those seconds during which the detector was in normal operating conditions and, in addition, AMS was pointing within 40° of the local zenith and the ISS was outside of the South Atlantic Anomaly. Because of the influence of the geomagnetic field, this collection time for galactic cosmic rays increases with rigidity becoming constant at 1.23×10^8 seconds above 30 GV.

Events are required to be downward going, to have a reconstructed track in the inner tracker, and to pass through $L1$. In the highest rigidity region, $R \geq 1.3$ TV, the track is also required to pass through $L9$. Track fitting quality criteria such as a $\chi^2/\text{d.o.f.} < 10$ in the bending coordinate are applied, similar to Refs. [12–14,24].

The measured rigidity is required to be greater than a factor of 1.2 times the maximum geomagnetic cutoff within the AMS field of view. The cutoff was calculated by backtracing particles from the top of AMS out to 50 Earth's radii [25] using the most recent IGRF [26] geomagnetic model.

Charge measurements on tracker $L1$, the inner tracker, the upper TOF, and, for $R \geq 1.3$ TV, tracker $L9$ are required to be compatible with charge $Z = 3$, 4, and 5, as shown in Fig. 1 of the Supplemental Material [21] for the inner tracker. With this selection, the charge confusion from noninteracted nuclei is negligible over the whole rigidity range. The residual background comes from heavier nuclei which interact above tracker $L2$. The background resulting from interactions in the material between $L1$ and $L2$ (TRD and upper TOF) is evaluated by fitting the charge distribution of tracker $L1$ with charge distribution templates of Li, Be, B, and C. Then cuts are applied on the $L1$ charge as shown in Fig. 2 of the Supplemental Material [21]. The charge distribution templates are obtained using L2. These templates contain only noninteracting events by requiring that $L1$ and $L3$–$L8$ measure the same charge value. This background is $< 0.5\%$ for lithium and beryllium and $< 3\%$ for boron. The background from interactions on materials above $L1$ (thin support structures made by carbon fiber and aluminum honeycomb) has been estimated from simulation using MC samples generated according to AMS flux measurements [14,21,27]. The simulation of nuclear interactions has been validated using data, as shown in Fig. 3 of the Supplemental Material [21]. For Li, Be, and B these backgrounds are estimated to be 5%, 8%, and 5% at 2 GV and 2%, 13%, and 8% at 3.3 TV, respectively. The uncertainties on the fluxes due to these background corrections were evaluated to be $< 1.5\%$ in the whole rigidity range.

Data analysis.— The isotropic flux Φ_i in the ith rigidity bin $(R_i, R_i + \Delta R_i)$ is given by

$$\Phi_i = \frac{N_i}{A_i \epsilon_i T_i \Delta R_i}, \tag{1}$$

where N_i is the number of events corrected for bin-to-bin migration, A_i is the effective acceptance, ϵ_i is the trigger efficiency, and T_i is the collection time. In this Letter the fluxes were measured in 67 bins from 1.9 GV to 3.3 TV with bin widths chosen according to the rigidity resolution and available statistics. The bins are identical for all nuclei and, except for the highest rigidity bin, also

identical with those used in our publication on the boron to carbon ratio [24].

The bin-to-bin migration of events was corrected using the unfolding procedure described in Ref. [12]. These corrections, $(N_i - \aleph_i)/\aleph_i$, where $\aleph_i$ is the number of observed events in bin i, are $+9\%$ at 3 GV, $+3\%$ at 5 GV, -5% at 150 GV, and -20% at 3.3 TV for lithium and very similar for beryllium and boron.

As discussed in Refs. [12–14,24], extensive studies were made of the systematic errors. These errors include the uncertainties in the two background estimations discussed above, the trigger efficiency, the geomagnetic cutoff factor, the acceptance calculation, the rigidity resolution function, and the absolute rigidity scale.

The systematic error on the fluxes associated with the trigger efficiency is $< 0.5\%$ over the entire rigidity range. The geomagnetic cutoff factor was varied from 1.0 to 1.4 resulting in a negligible systematic uncertainty (less than 0.1%) in the rigidity range below 30 GV.

The effective acceptances A_i were calculated using MC simulation and corrected for small differences between data and MC simulations related to (a) event reconstruction and selection, namely, in the efficiencies of velocity determination, track finding, charge determination, and tracker quality cuts and (b) the details of inelastic interactions of nuclei in the AMS materials. The total corrections to the effective acceptances from the differences between data and MC simulation were found to be $< 5\%$ over the entire rigidity range. The systematic errors on the fluxes associated with the reconstruction and selection are $< 2\%$ over the entire rigidity range for all nuclei. The material traversed by nuclei between $L1$ and $L9$ is composed primarily of carbon and aluminum, as described in detail in Ref. [13]. To verify the MC predictions, event samples that traverse materials between $L8$ and $L9$ (lower TOF and RICH) without interacting are measured in data and compared with MC samples simulated with inelastic cross sections varied within $\pm 10\%$. The resulting cross sections with the best agreement to data above 30 GV were chosen. Figure 4 of the Supplemental Material [21] shows the measured survival probabilities between $L8$ and $L9$ compared with simulation for lithium, beryllium, and boron. The survival probabilities are defined as the ratio of events which have the same charge value measured by $L1$–$L9$ to events which have the same charge value measured by $L1$–$L8$. Similarly, the survival probabilities between $L1$ and $L2$ have been calculated using data periods in which AMS was horizontal, i.e., $\sim 90°$ with respect to the zenith [13]. This independently verifies the inelastic cross sections. The systematic errors on the fluxes due to uncertainties of inelastic cross sections were evaluated to be $< 2\%$–3% up to 100 GV. At higher rigidities, the small rigidity dependencies of the cross sections from the Glauber-Gribov model were treated as uncertainties and added in quadrature to the uncertainties from the measured interaction probabilities. The resulting systematic errors on the fluxes were evaluated to be $< 3\%$–4% at 3.3 TV.

The rigidity resolution functions $\Delta(1/R)$ for Li, Be, and B have a pronounced Gaussian core characterized by width σ and non-Gaussian tails more than 2.5σ away from the center [13]. The resolution functions have been verified with the procedures described in detail in Ref. [24]. First, the differences of the coordinates measured in $L3$ or $L5$ to those obtained from the track fit using the measurements from $L1$, $L2$, $L4$, $L6$, $L7$, and $L8$ were compared between data and simulation. This procedure directly measures the tracker bending coordinate accuracy of 5.3–5.8 μm for Li, Be, and B, as shown in Fig. 5 of the Supplemental Material [21]. The comparisons for the tails of the distributions are shown in Fig. 6 of the Supplemental Material [21]. Second, the distributions of the scattering angle, defined as the angular difference between the inner tracker track and the $L1$ to $L2$ trajectory, were compared between data and simulation for Li, Be, and B and found to be in good agreement similar to Fig. SM 6 of Ref. [24]. This comparison verifies the multiple, nucleus-nucleus elastic, and quasielastic scatterings. The procedures provide the MDR of 3.5 TV for Li, 3.6 TV for Be, and 3.7 TV for B with 5% uncertainty and provide the uncertainties of 20% on the amplitudes of the non-Gaussian tails.

The systematic errors on the fluxes due to the rigidity resolution functions were obtained by repeating the unfolding procedure while varying the width of the Gaussian core of the resolution functions by 5% and by independently varying the amplitudes of the non-Gaussian tails by 20%. The resulting systematic errors on the fluxes are $< 1.5\%$ below 200 GV and increase to 8%–10% at 3.3 TV.

There are two contributions to the systematic uncertainty on the rigidity scale, discussed in detail in Ref. [12]. The first is due to residual tracker misalignment. This error was estimated by comparing the E/p ratio for electrons and positrons, where E is the energy measured with the ECAL and p is the momentum measured with the tracker. It was found to be $1/30$ TV^{-1} [28]. The second systematic error on the rigidity scale arises from the magnetic field map measurement and its temperature corrections. The error on the fluxes due to uncertainty on the rigidity scale is below 1% up to 200 GV and increases to 5%–7% at 3.3 TV.

Much effort has been spent to validate the systematic errors [12–14,24]. As an example, Fig. 7 of the Supplemental Material [21] shows the ratio of the measurements of the Li, Be, and B fluxes from 1.9 GV to 1.3 TV performed using events passing through $L1$ to $L8$ and using events passing through $L1$ to $L9$. The good agreement between the measurements verifies the systematic errors on unfolding, due to the difference in the resolution functions, as well as the systematic errors on acceptance, due to the difference in geometric factor and the amount of material traversed.

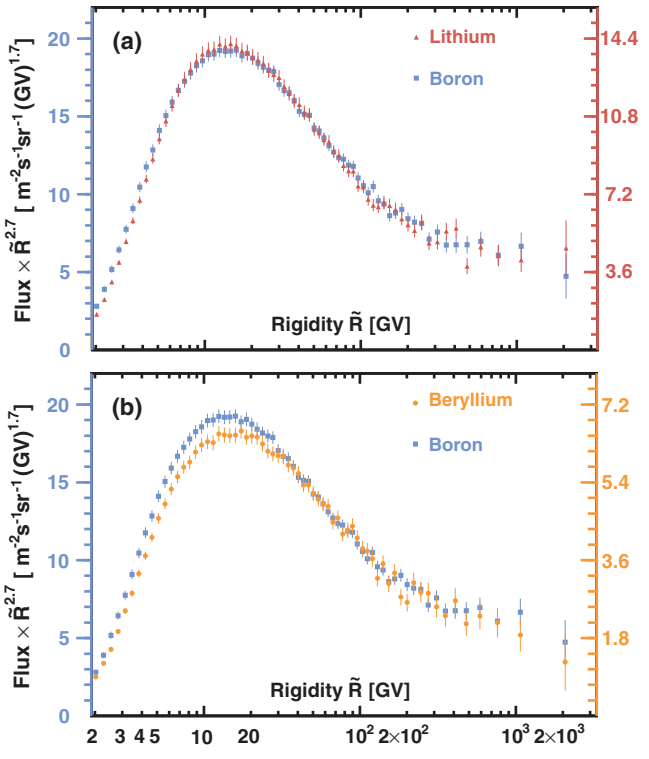

FIG. 1. The AMS (a) Li and B and (b) Be and B fluxes [21] multiplied by $\tilde{R}^{2.7}$ with their total errors as a function of rigidity. As seen, the Li and B fluxes have identical rigidity dependence above ∼7 GV and all three secondary fluxes have identical rigidity dependence above ∼30 GV.

Most importantly, several independent analyses were performed on the same data sample by different study groups. The results of those analyses are consistent with this Letter.

Results.— The measured lithium, beryllium, and boron fluxes including statistical and systematic errors are reported in Tables I, II, and III of the Supplemental Material [21] as a function of the rigidity at the top of the AMS detector.

Figure 1 shows the lithium, beryllium, and boron fluxes as a function of rigidity with the total errors, the sum in quadrature of statistical and systematic errors. In this and the subsequent figures, the points are placed along the abscissa at $\tilde{R}$ calculated for a flux $\propto R^{-2.7}$ [29]. As seen, the Li and B fluxes have an identical rigidity dependence above ∼7 GV and all three secondary fluxes have an identical rigidity dependence above ∼30 GV. The different rigidity dependence of the Be flux is most likely due to the significant presence of the radioactive ^{10}Be isotope [27], which has a half life of 1.4 MY.

Figure 8 of the Supplemental Material [21] shows the lithium, beryllium, and boron fluxes as a function of kinetic energy per nucleon E_K together with earlier measurements [2–11]. Data from other experiments have been extracted using Ref. [30]. For the AMS measurement $E_K = (\sqrt{Z^2\tilde{R}^2 + M^2} - M)/A$ where Z, M, and A are the Li, Be, and B charge, mass and atomic mass number, respectively. The atomic mass numbers, averaged by isotopic composition obtained from AMS low energy measurements [27], are 6.5 ± 0.1 for Li, 8.0 ± 0.2 for Be, and 10.7 ± 0.1 for B. The systematic errors on the fluxes due to these uncertainties were added in quadrature to the total errors.

To examine the rigidity dependence of the fluxes, detailed variations of the flux spectral indices with rigidity were obtained in a model-independent way. The flux spectral indices γ were calculated from

$$\gamma = d[\log(\Phi)]/d[\log(R)], \tag{2}$$

over rigidity intervals bounded by 7.09, 12.0, 16.6, 22.8, 41.9, 60.3, 192, and 3300 GV. The results are presented in Fig. 2 together with the spectral indices of helium, carbon, and oxygen [14]. As seen, the magnitude and the rigidity dependence of the lithium, beryllium, and boron spectral indices are nearly identical, but distinctly different from the rigidity dependence of helium, carbon, and oxygen. In addition, above ∼200 GV, Li, Be, and B all harden more than He, C, and O.

To examine the difference between the rigidity dependence of primary and secondary cosmic rays in detail, the ratios of the lithium, beryllium, and boron fluxes to the carbon and oxygen fluxes were computed using the data in Tables I, II, and III of the Supplemental Material [21] and Tables II and III of Ref. [14], and are reported in Tables IV–IX of the Supplemental Material [21] with their statistical and systematic errors. The detailed variations with rigidity of the spectral indices Δ of each flux ratio were obtained in a model independent way using

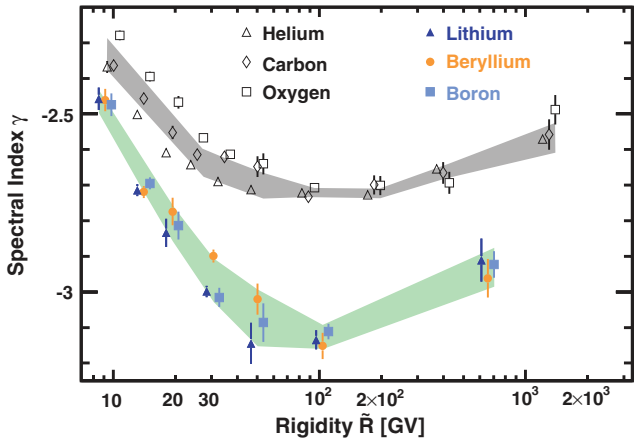

FIG. 2. The dependence of the Li, Be, and B spectral indices on rigidity together with the rigidity dependence of the He, C, and O spectral indices [14]. For clarity, the Li, B, He, and O data points are displaced horizontally. The shaded regions are to guide the eye. As seen, the magnitude and the rigidity dependence of the Li, Be, and B spectral indices are nearly identical, but distinctly different from the rigidity dependence of the He, C, and O spectral indices. Above ∼200 GV the Li, Be, and B fluxes all harden more than the He, C, and O fluxes. See also Fig. 3.

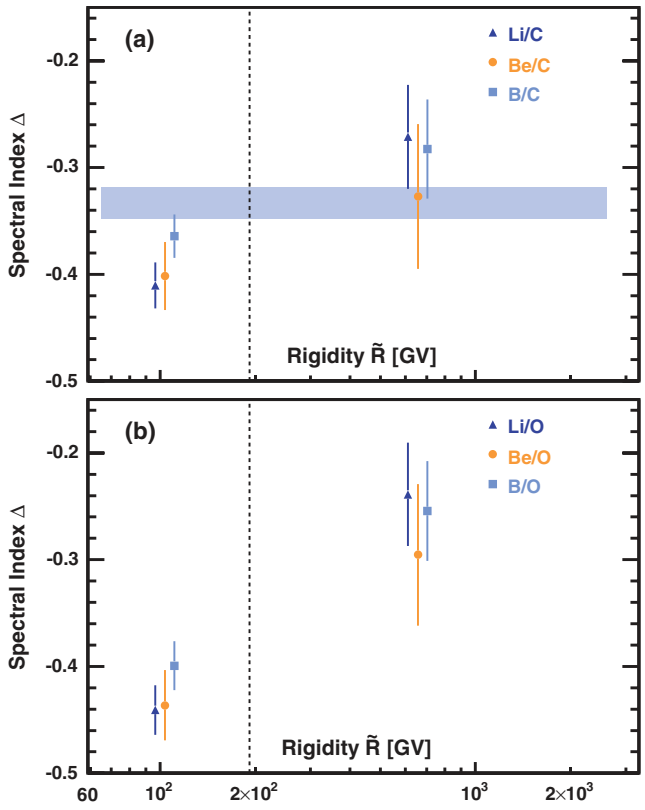

FIG. 3. The AMS secondary to primary flux ratio spectral indices Δ from Eq. (3) as functions of rigidity for (a) Li/C, Be/C, and B/C. The horizontal band indicates the fit to the B/C ratio from our previous publication [24] which is consistent with the results in this Letter. The results for (b) Li/O, Be/O, and B/O. For (a) and (b) the vertical dashed line shows the interval boundary. On average, the spectral indices of Li/C, Be/C, B/C, Li/O, Be/O, and B/O above 200 GV exhibit a hardening of 0.13 ± 0.03.

$$\Delta = d[\log(\Phi_S/\Phi_P)]/d[\log(R)], \tag{3}$$

where Φ_S/Φ_P are the ratios of the secondary to primary fluxes over rigidity intervals [60.3–192] and [192–3300] GV and shown in Fig 3. Above ~200 GV these spectral indices exhibit an average hardening of 0.13 ± 0.03. Figures 9 and 10 of the Supplemental Material [21] show all secondary to primary flux ratios together with the results of Eq. (3). This additionally verifies that at high rigidities the secondary cosmic rays harden more than the primary cosmic rays. This additional hardening of secondary cosmic rays is consistent with expectations when the hardening of cosmic ray fluxes is due to the propagation properties in the Galaxy [16].

To examine the rigidity dependence of the secondary cosmic rays in detail, the lithium to boron Li/B and beryllium to boron Be/B flux ratios were computed using the data in Tables I, II, and III of the Supplemental Material [21] and reported in Tables X and XI of the Supplemental Material [21] with their statistical and systematic errors. Figure 11 of the Supplemental Material [21] shows the (a) Li/B and (b) Be/B ratios as functions of rigidity with their total errors together with the results of fits to a constant

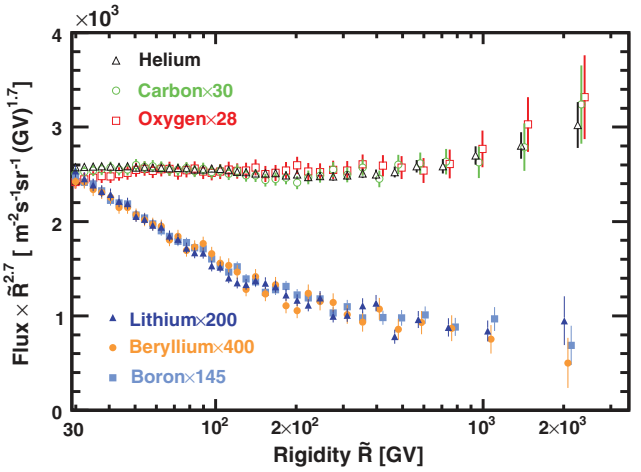

FIG. 4. Comparison of the secondary cosmic ray fluxes [21] with the AMS primary cosmic ray fluxes [14] multiplied by $\tilde{R}^{2.7}$ with their total error as a function of rigidity above 30 GV. For display purposes only, the C, O, Li, Be, and B fluxes were rescaled as indicated. For clarity, the He, O, Li, and B data points above 400 GV are displaced horizontally. As seen, the three secondary fluxes have an identical rigidity dependence above 30 GV, as do the three primary fluxes above 60 GV. The rigidity dependences of primary cosmic rays fluxes and of secondary cosmic rays fluxes are distinctly different.

value above 7 GV for Li/B and above 30 GV for Be/B. The fits yield $\mathrm{Li/B} = 0.72 \pm 0.02$ with $\chi^2/\mathrm{d.o.f.} = 51/53$ and $\mathrm{Be/B} = 0.36 \pm 0.01$ with $\chi^2/\mathrm{d.o.f.} = 27/35$. From these fits we note that the Li/Be ratio is 2.0 ± 0.1 above 30 GV; see also Fig. 12 of the Supplemental Material [21]. The Li and B fluxes have an identical rigidity dependence above ~7 GV and all three secondary fluxes have an identical rigidity dependence above ~30 GV. In Figs. 13, 14, and 15 of the Supplemental Material [21], we compare our flux ratios converted to E_K using the procedure described in Ref. [24] with earlier measurements [2–11,31–33].

In conclusion, we have presented precise, high statistics measurements of the lithium, beryllium, and boron fluxes from 1.9 GV to 3.3 TV with detailed studies of the systematic errors. The Li and B fluxes have identical rigidity dependence above 7 GV and all three fluxes have identical rigidity dependence above 30 GV with the Li/Be flux ratio of 2.0 ± 0.1. The three fluxes deviate from a single power law above 200 GV in an identical way. As seen in Fig. 4, this behavior of secondary cosmic rays has also been observed in primary cosmic rays He, C, and O [14] but the rigidity dependences of primary cosmic rays and of secondary cosmic rays are distinctly different. In particular, above 200 GV, the spectral indices of secondary cosmic rays harden by an average of 0.13 ± 0.03 more than the primaries. These are new properties of cosmic rays.

We thank former NASA Administrator Daniel S. Goldin for his dedication to the legacy of the ISS as a scientific

laboratory and his decision for NASA to fly AMS as a DOE payload. We also acknowledge the continuous support of the NASA leadership including Charles Bolden and William H. Gerstenmaier and of the JSC and Marshall Space Flight Center (MSFC) flight control teams which has allowed AMS to operate optimally on the ISS for over six years. We are grateful for the support of Jim Siegrist and his staff of the DOE including resources from the National Energy Research Scientific Computing Center under Contract No. DE-AC02-05CH11231 and the Argonne Leadership Computing Facility under Contract No. DE-AC02-06CH11357. We also acknowledge the continuous support from MIT and its School of Science, Michael Sipser, Marc Kastner, Ernest Moniz, Richard Milner, and Boleslaw Wyslouch. Research supported by São Paulo Research Foundation (FAPESP) Grants No. 2014/19149-7, No. 2015/50378-5, and No. 2016/10222-9, Brazil; CAS, NSFC, MOST, the provincial governments of Shandong, Jiangsu, Guangdong, and the China Scholarship Council, China; Action H2020 MSCA-IF-2015 under Grant No. 707543-MAtISSE, European Union; the Finnish Funding Agency for Innovation (Tekes) Grants No. 40361/01 and No. 40518/03 and the Academy of Finland Grant No. 258963, Finland; CNRS/IN2P3, CNES, Enigmass, and the ANR, France; Pascale Ehrenfreund, DLR under Grant No. 50OO1403 and JARA-HPC under Project No. JARA0052, Germany; INFN and ASI under ASI-INFN Agreements No. 2013-002-R.0 and No. 2014-037-R.0, Italy; CHEP and NRF under Grants No. NRF-2009-0080142 and No. NRF-2012-010226 at Kyungpook National University and No. NRF-2013-004883 at Ewha Womans University, Korea; the Consejo Nacional de Ciencia y Tecnología and UNAM, Mexico; FCT under Grant No. PTDC/FIS/122567/2010, Portugal; CIEMAT, IAC, CDTI, and SEIDI-MINECO under Grants No. ESP2015-71662-C2-(1-P/2-P), No. SEV-2015-0548, No. MDM-2015-0509, and No. RyC-2013-14660, Spain; the Swiss National Science Foundation (SNSF), federal and cantonal authorities, Switzerland; Academia Sinica and the Ministry of Science and Technology (MOST) under Grants No. 103-2112-M-006-018-MY3, No. 105-2112-M-001-003, and No. CDA-105-M06, former Presidents of Academia Sinica Yuan-Tseh Lee and Chi-Huey Wong and former Ministers of MOST Maw-Kuen Wu and Luo-Chuan Lee, Taiwan; the Turkish Atomic Energy Authority under Grant No. 2017TEAK(CERN)A5.H6.F2-15, Turkey; and NSF Grants No. 14255202 and No. 1551980, Wyle Laboratories Grant No. 2014/T72497, and NASA NESSF Grant No. HELIO15F-0005, USA. We gratefully acknowledge the strong support from CERN including Rolf-Dieter Heuer, Fabiola Gianotti, and the CERN IT department including Bernd Panzer-Steindel, and from the European Space Agency including Johann-Dietrich Wörner and Simonetta Di Pippo. We are grateful for important physics discussions with Fiorenza Donato, Jonathan Ellis, Jonathan Feng, Igor Moskalenko, Michael Salamon, Subir Sarkar, Joachim Trümper, Michael S. Turner, and Steven Weinberg.

[*]Also at ASI, I-00133 Roma, Italy.
[†]Also at ASI Space Science Data Center (SSDC), I-00133 Roma, Italy; Present address: University of Sassari, I-07100 Sassari, Italy.
[‡]Also at Wuhan University, Wuhan, 430072, China.
[§]Also at Sun Yat-Sen University (SYSU), Guangzhou, 510275, China.
[‖]Also at Huazhong University of Science and Technology (HUST), Wuhan, 430074, China.
[¶]Also at ASI Space Science Data Center (SSDC), I-00133 Roma, Italy.
[**]Also at ASI Space Science Data Center (SSDC), I-00133 Roma, Italy; Present address: INFN Sezione di Trieste, I–34149, Trieste, Italy.
[††]Also at Nankai University, Tianjin 300071, China.
[‡‡]Also at Institute of Theoretial Physics, Chinese Academy of Sciences, Beijing, 100190, China.

[1] I. A. Grenier, J. H. Black, and A. W. Strong, Annu. Rev. Astron. Astrophys. **53**, 199 (2015); P. Blasi, Astron. Astrophys. Rev. **21**, 70 (2013); A. W. Strong, I. V. Moskalenko, and V. S. Ptuskin, Annu. Rev. Nucl. Part. Sci. **57**, 285 (2007); A. Castellina and F. Donato, Astropart. Phys. **24**, 146 (2005).
[2] E. Juliusson, Astrophys. J. **191**, 331 (1974).
[3] C. D. Orth, A. Buffington, G. F. Smoot, and T. S. Mast, Astrophys. J. **226**, 1147 (1978).
[4] W. R. Webber and S. M. Yushak, *Proceedings of 16th International Cosmic Ray Conference, Tokyo* (Institute for Cosmic Ray Research, Univ. of Tokyo, Tokyo, Japan, 1979), Vol. 12, p. 51.
[5] J. A. Lezniak and W. R. Webber, Astrophys. J. **223**, 676 (1978).
[6] J. J. Engelmann, P. Ferrando, A. Soutoul, P. Goret, and E. Juliusson, Astron. Astrophys. **233**, 96 (1990).
[7] R. C. Maehl, J. F. Ormes, A. J. Fisher, and F. A. Hagen, Astrophys. Space Sci. **47**, 163 (1977).
[8] M. Simon, H. Spiegelhauer, W. K. H. Schmidt, F. Siohan, J. F. Ormes, V. K. Balasubrahmanyan, and J. F. Arens, Astrophys. J. **239**, 712 (1980).
[9] S. P. Swordy, D. Müller, P. Meyer, J. L'Heureux, and J. M. Grunsfeld, Astrophys. J. **349**, 625 (1990).
[10] A. Obermeier, M. Ave, P. Boyle, Ch. Höppner, J. Hörandel, and D. Müller, Astrophys. J. **742**, 14 (2011).
[11] O. Adriani *et al.*, Astrophys. J. **791**, 93 (2014).
[12] M. Aguilar *et al.*, Phys. Rev. Lett. **114**, 171103 (2015).
[13] M. Aguilar *et al.*, Phys. Rev. Lett. **115**, 211101 (2015).
[14] M. Aguilar *et al.*, Phys. Rev. Lett. **119**, 251101 (2017).
[15] P. L. Biermann, J. K. Becker, J. Dreyer, A. Meli, E.-S. Seo, and T. Stanev, Astrophys. J. **725**, 184 (2010); Y. Ohira and K. Ioka, Astrophys. J. Lett. **729**, L13 (2011); Q. Yuan, B. Zhang, and X.-J. Bi, *Proceedings of the 32nd International Cosmic Ray Conference, Beijing* (Institute of High Energy Physics, Beijing, 2011), Vol. 6, p. 222; S. Thoudam and J. R. Hörandel, Mon. Not. R. Astron. Soc. **435**, 2532 (2013).
[16] S. Thoudam and J. R. Hörandel, Astron. Astrophys. **567**, A33 (2014); P. Blasi, E. Amato, and P. D. Serpico, Phys. Rev. Lett. **109**, 061101 (2012); N. Tomassetti, Phys. Rev. D **92**, 081301 (R) (2015); A. E. Vladimirov, G. Jóhannesson, I. V. Moskalenko, and T. A. Porter, Astrophys. J. **752**, 68 (2012).
[17] A. Kounine, Int. J. Mod. Phys. E **21**, 1230005 (2012); S. Rosier-Lees, *Proceedings of Astroparticle Physics TEVPA/*

IDM, Amsterdam (2014); S. Ting, Nucl. Phys. B, Proc. Suppl. **243–244**, 12 (2013); S.-C. Lee, Proceedings of the 20th International Conference on Supersymmetry and Unification of Fundamental Interactions (SUSY 2012), Beijing, 2012 (unpublished); M. Aguilar, Proceedings of the XL International Meeting on Fundamental Physics, Centro de Ciencias de Benasque Pedro Pascual, 2012 (unpublished); S. Schael, Proceedings of the 10th Symposium on Sources and Detection of Dark Matter and Dark Energy in the Universe, Los Angeles, 2012 (unpublished); B. Bertucci, *Proc. Sci.*, EPS-HEP, (2011) 67; M. Incagli, AIP Conf. Proc. **1223**, 43 (2010); R. Battiston, Nucl. Instrum. Methods Phys. Res., Sect. A **588**, 227 (2008).

[18] K. Lübelsmeyer *et al.*, Nucl. Instrum. Methods Phys. Res., Sect. A **654**, 639 (2011).

[19] B. Alpat *et al.*, Nucl. Instrum. Methods Phys. Res., Sect. A **613**, 207 (2010).

[20] V. Bindi *et al.*, Nucl. Instrum. Methods Phys. Res., Sect. A **743**, 22 (2014), and references therein.

[21] See Supplemental Material at http://link.aps.org/supplemental/10.1103/PhysRevLett.120.021101 for details of the AMS detector; for the tabulated lithium, beryllium, and boron fluxes as functions of rigidity; for the tabulated Li/C, Be/C, B/C, Li/O, Be/O, B/O, Li/B, and Be/B flux ratios as functions of rigidity; and for figures related to the charge selection and systematic errors, of the fluxes as functions of kinetic energy per nucleon E_K together with earlier measurements, of the eight flux ratios as functions of rigidity, of a comparison of the Li and Be flux, and of the eight flux ratios as functions of kinetic energy per nucleon E_K together with earlier measurements.

[22] G. Ambrosi, V. Choutko, C. Delgado, A. Oliva, Q. Yan, and Y. Li, Nucl. Instrum. Methods Phys. Res., Sect. A **869**, 29 (2017). With large samples of nuclei data, we are able to accurately account for nonlinear saturation effects in the tracker lectronics and this has improved the AMS tracker coordinate resolution for nuclei.

[23] J. Allison *et al.*, Nucl. Instrum. Methods Phys. Res., Sect. A **835**, 186 (2016); S. Agostinelli *et al.*, Nucl. Instrum. Methods Phys. Res., Sect. A **506**, 250 (2003).

[24] M. Aguilar *et al.*, Phys. Rev. Lett. **117**, 231102 (2016).

[25] J. Alcaraz *et al.*, Phys. Lett. B **484**, 10 (2000).

[26] C. C. Finlay *et al.*, Geophys. J. Int. **183**, 1216 (2010); E. Thébault *et al.*, Earth Planets Space **67**, 79 (2015).

[27] AMS Collaboration, Measurement of cosmic ray fluxes with the alpha magnetic spectrometer on the international space station (to be published).

[28] J. Berdugo, V. Choutko, C. Delgado, and Q. Yan, Nucl. Instrum. Methods Phys. Res., Sect. A **869C**, 10 (2017).

[29] G. D. Lafferty and T. R. Wyatt, Nucl. Instrum. Methods Phys. Res., Sect. A **355**, 541 (1995). We have used Eq. (6) with $\tilde{R} \equiv x_{lw}$.

[30] D. Maurin, F. Melot, and R. Taillet, Astron. Astrophys. **569**, A32 (2014).

[31] M. Aguilar *et al.*, Astrophys. J. **724**, 329 (2010).

[32] H. S. Ahn *et al.*, Astropart. Phys. **30**, 133 (2008).

[33] A. D. Panov *et al.*, *Proceedings of the 30th International Cosmic Ray Conference, Mérida* (Universidad Autónoma de Yucatán, Mérida, 2008), Vol. 2, p. 3.